



# Energy performance of phase change materials integrated into brick masonry walls for cooling load management in residential buildings

Aakash C. Rai

*Department of Mechanical Engineering, Birla Institute of Technology and Science, Pilani, Rajasthan, 333031, India*



## ARTICLE INFO

**Keywords:**

Phase change material  
Insulation  
Night ventilation  
Wall heat transfer  
Energy-efficient buildings  
Numerical simulations

## ABSTRACT

Energy demand for space cooling in residential buildings is projected to witness rapid growth, primarily fueled by increasing household incomes in developing countries. To manage this ever-increasing cooling demand, integration of phase change materials (PCMs) in building walls is a potential solution that can reduce the buildings' cooling energy consumption and peak cooling loads. However, to attain the proposed benefits from PCM integration, it is crucial to appropriately select PCM parameters such as its phase-change temperature and positioning in the wall. Thus, this investigation studied the energy performance of PCM integrated brick masonry walls for cooling load management in residential buildings under periodic steady-state conditions to identify the parameters that govern its performance and develop simple design guidelines.

The research found that regardless of the amount of latent heat stored by the PCM, the daily heat gains and cooling loads were equal for wall configurations having equal thermal resistances under identical boundary conditions. Furthermore, even with the application of night ventilation, adding a PCM layer to a well-insulated wall did not reduce its cooling load; thus, PCM integration was ineffective in reducing the cooling load. However, the latent heat stored by the PCM reduced the fluctuations in the hourly heat gains and cooling loads; thus, PCM integration was found suitable for peak load management. For the PCM's proper utilization, its recommended position is on the inner side of the wall with sufficient insulation shielding it from outdoor conditions, and its melting temperature should be close to the indoor set-point temperature.

## 1. Introduction

Residential buildings account for about 24% of the global energy consumption, of which roughly 2% is used for space cooling [1]. The residential cooling energy use is projected to increase rapidly in the future (from close to 300 TWh in 2000 to about 4000 TWh in 2050 and more than 10,000 TWh in 2100), primarily fueled by increasing household incomes in developing countries like India and China [2]. For managing the increasing space cooling needs, integration of phase change materials (PCMs) in the building envelope is a potential solution for improving the energy efficiency of new and existing buildings [3–8]. PCMs work on the principle of latent heat thermal energy storage. During periods of high heat gains (day-time), they undergo phase transformation (typically solid to liquid) and store the excess thermal energy, which is released back during periods of low heat gains (night-time). By this process, they seem to reduce the cooling energy consumption, peak cooling loads, and delay the peak loads to later hours. However, for their proper functioning, it is crucial to appropriately select PCM parameters such as its phase-change temperature (or

melting temperature for a solid-liquid transformation) and position in the building envelope [9,10].

### 1.1. Research on PCM integration into lightweight walls

External walls contribute significantly to heat gains in residential buildings, and through their energy-efficient design, the buildings' cooling energy requirements can be substantially lowered [11–14]. Thus, several investigations have experimentally studied the potential of PCMs integrated into external building walls for peak load management and for reducing the seasonal/annual energy consumption in air-conditioned buildings [15,16]. For example, Medina and co-workers conducted a series of experiments to assess the energy performance of typical lightweight wall assemblies enhanced with PCMs in North-American residences under summer conditions. They developed a 'dynamics wall simulator' and studied the energy performance of different PCM integration techniques in walls [17–19]. Those studies found that due to PCM integration, peak heat fluxes were reduced by as much as 9.2%–36.5%, while reductions in daily heat gains ranged from 1.01 W h m<sup>-2</sup>–51.2 W h m<sup>-2</sup>, as compared to the baseline wall. Those

E-mail address: [aakash.rai@pilani.bits-pilani.ac.in](mailto:aakash.rai@pilani.bits-pilani.ac.in).

Nomenclature	
A	wall area, $\text{m}^2$
ACR	air change rate for night ventilation, $\text{h}^{-1}$
C	specific heat capacity, $\text{J}\cdot\text{kg}^{-1}\cdot\text{C}^{-1}$
DBT	dry bulb temperature
EPS	expanded polystyrene
h	heat transfer coefficient, $\text{W}\cdot\text{m}^{-2}\cdot\text{C}^{-1}$
H	wall height, m
i	enthalpy, $\text{J}\cdot\text{kg}^{-1}$
I	incident solar radiation, $\text{W}\cdot\text{m}^{-2}$
NV	night ventilation
PCM	phase change material
q	heat flux, $\text{W}\cdot\text{m}^{-2}$
r <sub>j</sub>	jth radiant time factor, dimensionless
R	daily temperature range, $^\circ\text{C}$
RTSM	radiant time series method
RTF	radiant time factor
t	time, s
T	temperature, $^\circ\text{C}$
U	overall heat transfer coefficient, $\text{W}\cdot\text{m}^{-2}\cdot\text{C}^{-1}$
V	room air volume, $\text{m}^3$
̇V	night ventilation rate, $\text{m}^3\cdot\text{s}^{-1}$
x	space coordinate, m
X <sub>n</sub>	temperature range multiplier, dimensionless
<i>Greek symbols</i>	
$\alpha$	solar absorptivity, dimensionless
$\lambda$	thermal conductivity, $\text{W}\cdot\text{m}^{-1}\cdot\text{C}^{-1}$
$\rho$	density, $\text{kg}\cdot\text{m}^{-3}$
<i>Subscripts</i>	
air	air
avg	average value
con	convective component of the heat gain
CL	wall cooling load
eq	equivalent value
HG	wall heat gain at its interior surface
in	indoor
n	value at the nth hour
new	value at the current time step
old	value at the previous time step
out	outdoor
rad	radiative component of the heat gain
sol-air	solar air
tot	total over 24 h

studies were extended by constructing two identical scale models of typical North-American houses and comparing the energy performance of PCM-enhanced walls with conventional ones [20–23]. Once more, PCM integration in walls significantly reduced the peak heat fluxes and the total heat gains during summers.

Similar to the abovementioned experimental studies, several numerical studies have also been conducted to assess the potential benefits of PCM integration in lightweight residential walls for cooling load management [24–33]. For example, Lee and Medina [27] used EnergyPro software to study the performance of wood-frame walls containing PCMs in coastal and transitional climates of California. They found that as compared to the conventional construction, PCM-outfitted walls reduced the cooling load by about 10.4%, while reductions in peak wall heat fluxes ranged between 2.2% and 32.4% depending on the wall orientation, climate zone, and PCM amount. Another investigation by Zwanzig et al. [30] conducted numerical simulations to study the energy performance of a PCM composite wallboard placed in different locations within a residential wall for three different climate zones in the USA. The study found that using PCM composite wallboards (with suitable phase change temperature of the PCM) can substantially decrease and delay the peak cooling loads. The reductions in cooling energy ranged from as low as 0.02% for an east-facing wall in Miami, Florida (coastal climate) to as high as 38.25% for a south-facing wall in Minneapolis, Minnesota (cold climate); thus highlighting the necessity to choose different PCMs for different climate zones. Soares et al. [29] evaluated the impact of PCM integration in walls on the cooling energy consumption of an air-conditioned lightweight steel-framed residential building under seven different European climates. They also found that by integrating PCM in the external walls, the cooling energy consumption of the building could be reduced by 43%–87% depending on the climatic conditions.

## 1.2. Research on PCM integration into heavyweight walls

In contrast to several studies available on the integration of PCMs in lightweight walls, relatively few studies have evaluated the energy benefits of PCM integration into heavyweight walls [34–40]. For instance, Ascione et al. [34] studied PCM-based refurbishment strategies for heavyweight buildings (post-world-war reinforced concrete

construction in Europe) in Mediterranean countries under hot summer conditions using numerical simulations. They found that PCM-based refurbishments reduced the cooling energy consumption by about 7.2% in a semi-arid climate (Ankara, Turkey). In contrast, cooling energy savings were less than 4.1% in cities with warm/hot Mediterranean sub-tropical climates. Another study by Lei et al. [37] reported that PCMs integrated into heavyweight concrete walls reduced the heat gains by 21%–32% throughout the whole year in the tropical climate conditions of Singapore. They also demonstrated that with the proper selection of PCM's phase change temperature, the PCM applied to the external wall surface could undergo complete melting-solidification cycles despite the low variations in the daily ambient temperatures (5  $^\circ\text{C}$ –7  $^\circ\text{C}$ ). This happens because solar radiations heat the exterior walls to temperatures up to 42  $^\circ\text{C}$  during the day, while the walls cool down during the night to temperatures as low as 23  $^\circ\text{C}$ , thus providing the required temperature variation for the PCM to complete its melting-solidification cycle. A similar conclusion was also obtained by Saxena et al. [41], who studied the suitability of three commercially available PCMs for cooling load reductions in New Delhi (composite climate), and recommended a phase change temperature of 34  $^\circ\text{C}$  for the PCM to undergo efficient melting-solidification cycles.

## 1.3. Research gaps and aims of the present study

The above discussion shows that integration of PCMs into walls could be an effective technique for cooling load management in residential buildings; however, the following gaps in knowledge remain that motivate the present investigation:

- Most existing studies have calculated cooling energy savings by comparing PCM-enhanced walls with those without PCMs; thus, the reported energy benefits were not only because of an increase in the thermal mass of the wall but also because of an increase in its thermal resistance. For example, due to PCM integration, the wall's thermal resistance increased by as much as 10.7% in Ascione et al. [34], by as much as 16.2% in Soares et al. [39], and by up to 63.2% in Lei et al. [37] since PCM materials typically have low thermal conductivities. Thus, actual energy savings due to the thermal mass effect of the PCM will be significantly lower than those generally reported in the

literature, as highlighted by a few studies [30,42,43]. Furthermore, to convincingly demonstrate the benefits of PCM-based enhancements, their energy performance should be compared with other cheaper energy-efficiency solutions such as insulation. A few investigations that have compared PCM-enhanced envelopes with those enhanced with insulation have reported that insulated envelopes outperformed those with PCMs [35,44]. The present study dealt with those issues by comparing the performances of PCM-enhanced walls with walls enhanced with insulation while maintaining equal thermal resistance.

- Another issue with existing studies is that their results cannot be interpreted easily due to the dynamic nature of the experiments and simulations [34], which leads to variations in indoor and outdoor conditions each day, making it challenging to identify the parameters that govern the PCM layer's performance. However, the present investigation compared PCM-enhanced walls with insulated ones for typical summer days under periodic steady-state conditions to identify the parameters that affect the performance of PCM-enhanced walls and develop simple design guidelines.

## 2. Methodology

### 2.1. System description

This investigation evaluated the benefits of PCM integration in heavyweight residential building walls for cooling load management in India since such buildings are likely to see tremendous growth in cooling energy demand due to increasing household incomes in India [45]. The different wall configurations studied are illustrated in Fig. 1, and the thermophysical properties of the different layers of the wall construction are given in Table 1. As shown in Fig. 1, the standard brick masonry wall (termed as Brick wall) is made of solid clay-fired bricks with cement plaster applied on both sides. This wall consists of individual bricks arranged in a systematic order and bound together by cement mortar, which means that the thermophysical properties of mortar will modify the effective properties of this layer. However, the thermophysical properties (density = 1600–1635 kg m<sup>-3</sup>, thermal conductivity = 0.75–0.97 W m<sup>-1</sup> °C<sup>-1</sup>, specific heat = 1050 J kg<sup>-1</sup> °C<sup>-1</sup>) of cement mortar [46,47] are similar to those of solid clay-fired bricks (see Table 1). Thus, this investigation assumed that the effective thermophysical properties of the brick layer were well represented by those of clay-fired bricks only.

For enhancing the standard wall, a 150 mm thick expanded polystyrene (EPS) insulation layer was applied on the inner (Brick-EPS) or the outer side (EPS-Brick) of the wall, which increased its thermal resistance from 0.3 m<sup>2</sup> K.W<sup>-1</sup> to 4.6 m<sup>2</sup> K.W<sup>-1</sup>. This investigation further studied six more configurations with a 10 mm thick PCM layer

positioned in different arrangements, as shown in Fig. 1. The PCM layer thickness was taken as 10 mm since some previous researchers have recommended this as the optimum thickness [48,49]. Furthermore, a 10 mm thick PCM layer provided a significant latent heat capacity (1800 kJ m<sup>-2</sup>) without adding considerably to the wall's thermal resistance. The PCM layer was integrated into the wall in a 'passive' manner, i.e., the phase-change process occurs due to the natural variations in the wall temperature throughout the day, without the aid of any mechanical equipment. In configurations with PCM, the insulation layer's thickness was reduced slightly (from 150 mm to 147.7 mm) to keep the thermal resistance equal between the insulated walls (EPS-Brick and Brick-EPS) and those containing both insulation and PCM.

The PCM studied was a paraffin-based PCM (RT from Rubitherm) with a very high latent heat capacity to maximize the effect of thermal energy storage, whose thermophysical properties are given in Table 1, as reported by its manufacturer. The PCM's melting temperature was varied, depending on the configuration under study, such that the PCM undergoes melting and solidification cycles. It was assumed that the PCM had the same thermophysical properties both in its solid and liquid phase, which was reasonable since the properties of paraffin-based PCMs do not markedly vary between the solid and the liquid phase for the narrow temperature range of operation used in this investigation [50]. It was also assumed that the PCM material was attached directly to the wall, which means that the effect of any container holding the PCM was neglected. The phase transformation of the PCM was assumed to take place over a 2 °C temperature range centered around the melting temperature, as illustrated in the enthalpy-temperature profile of the PCMs given in Fig. 2. Thus, the PCMs studied in this investigation were idealized versions of Rubitherm's RT range of PCMs, designed to understand the role of PCM's phase change temperature on the proposed energy benefits.

### 2.2. Mathematical formulation

To investigate the heat transfer through the different wall constructions described above, this investigation conducted a 1-dimensional transient heat conduction analysis using the CondFD algorithm in EnergyPlus (version 9.0.1) software [51]. This research simulated the periodic (a series of days, all having the same hourly variations in the outdoor conditions) steady-state behavior of the one-dimensional heat conduction through the walls as governed by:

$$\rho C \frac{\partial T}{\partial t} = \lambda \frac{\partial^2 T}{\partial x^2} \quad (1)$$

where  $T$  denotes the wall temperature, which is a function of space ( $x$ ) and time ( $t$ ); and  $\rho$ ,  $C$ , and  $\lambda$  denote the material density, specific heat, and thermal conductivity values, respectively.

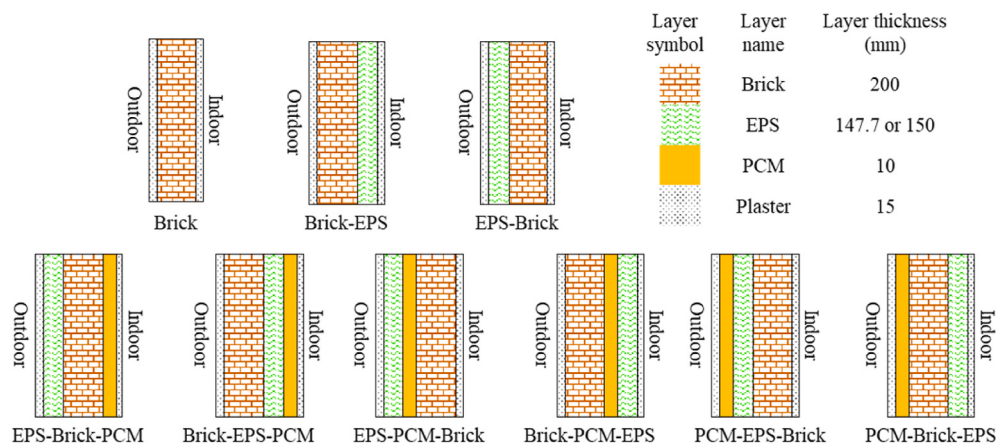
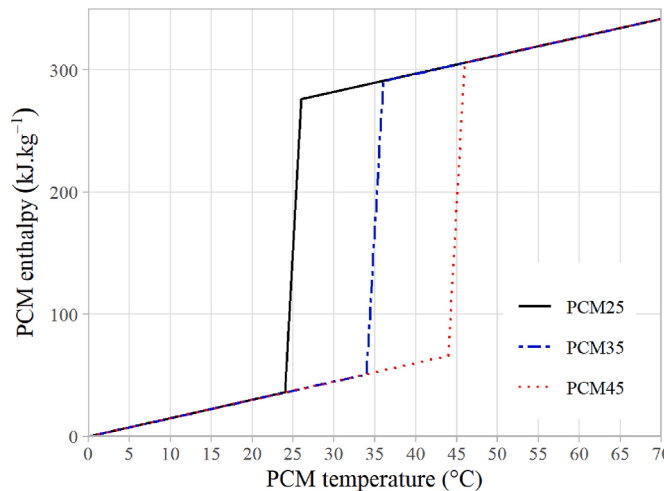


Fig. 1. Schematics of different wall constructions (layer thickness is not to scale). The layers (Brick, EPS, and PCM) are ordered, starting from outdoors to indoors.

**Table 1**

Thermophysical properties of the different layers of the wall construction.

Layer	Thickness (mm)	Density ( $\text{kg.m}^{-3}$ )	Thermal conductivity ( $\text{W.m}^{-1}\text{.}^{\circ}\text{C}^{-1}$ )	Specific heat ( $\text{J.kg}^{-1}\text{.}^{\circ}\text{C}^{-1}$ )	Latent heat ( $\text{kJ.kg}^{-1}$ )
Cement plaster	15	1300	0.5	1000	–
Clay-fired bricks	200	1700	0.84	800	–
Insulation (EPS)	147.7 or 150	24	0.035	1340	–
PCM (RT from Rubitherm)	10	750	0.15	1500	240



**Fig. 2.** Enthalpy versus temperature diagram for some representative PCMs. The digits in legend after PCM represent its melting temperature (°C).

For solving Eq. (1), the boundary condition at the interior surface of the wall ( $x = x_{in}$ ) was

$$-\lambda \frac{\partial T}{\partial x} \Big|_{x=x_{in}} = h_{in}(T_{x=x_{in}} - T_{in}) \quad (2)$$

where  $h_{in}$  is the combined convective and radiative heat transfer coefficient between the surface and indoor air, and  $T_{in}$  is the indoor air dry bulb temperature (DBT). To simplify the model,  $h_{in} = 8.3 \text{ W m}^2 \text{ }^{\circ}\text{C}^{-1}$  was used that is suitable for vertical walls with horizontal direction of heat transfer under still air conditions [47].

For the exterior wall surface ( $x = x_{out}$ ), the following boundary condition was applied:

$$-\lambda \frac{\partial T}{\partial x} \Big|_{x=x_{out}} = I\alpha - h_{out}(T_{x=x_{out}} - T_{out}) \quad (3)$$

where  $I$  is the incident solar radiation,  $\alpha$  the solar absorptivity,  $h_{out}$  the combined convective and radiative heat transfer coefficient between the surface and outdoor air, and  $T_{out}$  the outdoor air DBT. Note that Eq. (3) was simplified by assuming a constant  $h_{out}$  as:

$$-\lambda \frac{\partial T}{\partial x} \Big|_{x=x_{out}} = h_{out}(T_{sol-air} - T_{x=x_{out}}) \quad (4)$$

where  $T_{sol-air}$  denotes the hourly sol-air temperature, and calculated from the hourly values of outdoor air DBT ( $T_{out}$ ) and incident solar radiation ( $I$ ) by using:

$$T_{sol-air} = T_{out} + \frac{I\alpha}{h_{out}} \quad (5)$$

Due to these simplifications, the wall heat transfer was governed only by  $T_{in}$  (a constant value of 26 °C was used), and  $T_{sol-air}$  (varies through the day due to variations in the outdoor DBT and incident solar radiation on the wall). This model has the inherent advantage of reducing the number of independent variables that affect the wall heat transfer, while keeping the model realistic enough for identifying the

physical parameters that impact the heat transfer through different wall configurations.

For simulating cases with PCM, Eq. (1) was accompanied by another equation that defines the relationship between the PCM's enthalpy and its temperature:

$$i = i(T) \quad (6)$$

where  $i$  and  $T$  are the enthalpy and temperature of the PCM, respectively.

The enthalpy-temperature relation, as shown in Fig. 2, was used to compute an equivalent specific heat at each time-step to account for the enthalpy change during the phase change process, which is given by:

$$C_{eq} = \frac{i_{new} - i_{old}}{T_{new} - T_{old}} \quad (7)$$

where  $C_{eq}$  is the equivalent specific heat capacity of the PCM, and the subscripts,  $new$  and  $old$ , refer to the values of the variables at the current and the previous time steps, respectively.

### 2.3. Cooling load calculations

The simulation output from EnergyPlus only gave hourly heat gains through the walls, but not the cooling loads since a combined value of the indoor convective and radiative heat transfer coefficient ( $h_{in}$  in Eq. (2)) was used to simplify the model for the reasons mentioned above. Thus, for obtaining the hourly cooling loads, this investigation used the radiant time series method (RTSM) to estimate cooling loads from hourly values of heat gains and details of the building construction [47].

For applying this method, the building was assumed to be an air-conditioned room (dimensions: 3.64 m × 3.64 m × 2.75 m) with standard brick walls (Brick configuration shown in Fig. 1) and a concrete roof and floor. Next, the hourly wall heat gains (EnergyPlus output) were split into their convective and radiative portions, assumed to be 37% and 63%, respectively, as specified by the RTSM method. At any hour, the convective heat gains immediately contribute to the cooling load, while contributions of the radiant heat gains are determined based on their current and past values. Thus, the hourly cooling load is given by:

$$\dot{q}_{CL,n} = \dot{q}_{con,n} + r_0 \dot{q}_{rad,n} + r_1 \dot{q}_{rad,n-1} + r_2 \dot{q}_{rad,n-2} + \dots + r_{23} \dot{q}_{rad,n-23} \quad (8)$$

where  $\dot{q}_{CL,n}$  ( $\text{W.m}^{-2}$ ) is the wall cooling load at the nth hour,  $\dot{q}_{con,n}$  ( $\text{W.m}^{-2}$ ) the convective portion of the heat gain at that hour,  $\dot{q}_{rad,n-j}$  ( $\text{W.m}^{-2}$ ) the radiant portion of the heat gain  $j$  hours ago ( $j$  denotes the time lag between the cooling load and the radiant heat gain and varies from 0 to 23), and  $r_j$  the  $j$ th radiant time factor (RTF). The RTFs (given in Fig. SI 1 in supplementary material) were estimated from the details of the room construction by using the procedure described by Spitler et al. [52].

This method made it possible to calculate the cooling load requirements corresponding to the different wall configurations, as if that wall was part of a small room and exposed to the outdoor conditions. This method did not account for the cooling load due to heat gains through doors, roof, glazing, infiltration, and internal heat sources. Nevertheless, the estimated cooling loads corresponding to the wall heat gains will be reasonable for a small air-conditioned zone of heavyweight construction since the zone's thermal inertia (product of mass and

specific heat) mainly governs the conversion of heat gains to cooling loads. Note that since the heat gains were independent of the zone's construction, those results have a broader applicability than the reported cooling loads.

#### 2.4. Night ventilation calculations

This investigation also studied the potential of night ventilation for reducing the total daily cooling loads. The study assumed that night ventilation was activated (at a sufficient ventilation rate) whenever the outdoor DBT dropped below the indoor set-point temperature (DBT = 26 °C), and the 'free' cooling provided by it entirely offset the wall's cooling load for that hour. This meant that the wall's cooling load was zero when night ventilation was active. The required night ventilation rate was calculated using a simple energy balance:

$$\dot{q}_{CL,n}A = \dot{V}\rho_{air}C_{air}(T_{in} - T_{out}) \quad (9)$$

where  $\dot{q}_{CL,n}$  is the wall cooling load at the nth hour,  $A$  the wall area,  $\dot{V}$  the night ventilation rate;  $T_{in}$  and  $T_{out}$  the indoor and outdoor air DBTs, respectively, and  $\rho_{air}$  and  $C_{air}$  the density and heat capacity of air, respectively.

The above equation was rearranged to compute the required air change rate for night ventilation as:

$$ACR = \frac{\dot{V}}{V} = \frac{\dot{q}_{CL,n}}{H\rho_{air}C_{air}(T_{in} - T_{out})} \quad (10)$$

where  $ACR$  is the required air change rate ( $\text{h}^{-1}$ ) for night ventilation,  $V$  the air volume inside the room, and  $H$  the wall height ( $H = V/A$ ).

#### 2.5. Model inputs

This study simulated walls facing all four cardinal directions (east, west, north, and south) with four different hourly profiles of the outdoor air DBT, as shown in Fig. 3. Those hourly profiles were generated by taking two representative values for the daily average DBT ( $T_{out,avg} = 26^\circ\text{C}$  or  $32^\circ\text{C}$ ) and two for the daily DBT range ( $R = 6^\circ\text{C}$  or  $12^\circ\text{C}$ ), and by using the following equation:

$$T_{out,n} = \left( T_{out,avg} + \frac{R}{2} \right) - X_n(R) \quad (11)$$

where  $T_{out,n}$  represents the outdoor temperature at the nth hour, and  $X_n$  is the temperature range multiplier (between 0 and 1) for that hour whose values were taken from ASHRAE's handbook [53].

The generated DBT profiles were labeled as T32R12, T32R6, T26R12, and T26R6, where the numbers after "T" indicate the average

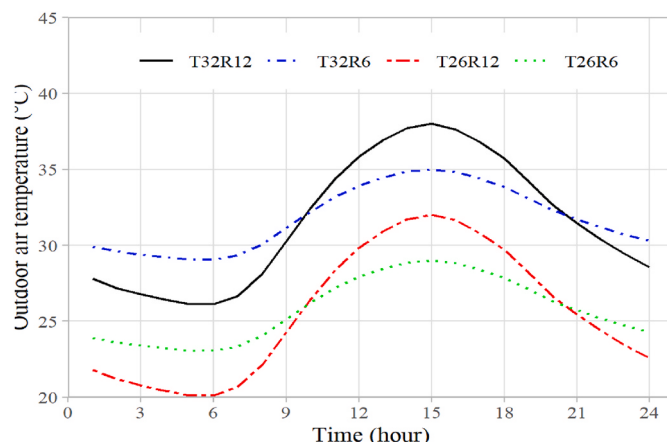


Fig. 3. Hourly variation of outdoor air DBT with time.

DBT value, and those after "R" indicate the daily DBT range. Those DBT profiles can represent a wide range of summer conditions. For example, T32R6 or T26R6 could represent a hot or mild day in a coastal location (low daily temperature variation), while T32R12 or T26R12 could represent hot or mild summer days in an arid location (high daily temperature variation). The solar radiation incident on the walls was obtained from the ASHRAE Tau 2017 model (revised clear sky model) for a summer day (21st May), assuming the location to be New Delhi (latitude = 28.585° N, longitude = 77.206° E). As discussed previously, this investigation combined the effects of outdoor DBT and incident solar radiation into an equivalent sol-air temperature by using Eq. (5). The sol-air temperature profiles ( $4 \times 4 = 16$  unique profiles) for the four cardinal directions subjected to all four outdoor DBT conditions are shown in Fig. SI 2.

#### 2.6. Model validation

EnergyPlus software used in this investigation has been extensively validated for energy simulation in building walls containing PCMs [54]. This investigation followed all the recommendations of the previous studies and also conducted additional tests to validate the model. Those test details are given in the following sub-sections, and the final solver settings used in this investigation are presented in Table SI 1.

##### 2.6.1. Comparison of numerical results with the analytical solution of Stefan's problem

Stefan's problem studies the melting process in a 1-dimensional PCM that is initially solid and at a uniform temperature equal to its melting temperature. The PCM temperature at one end is raised suddenly to a constant value such that the melting process starts from that end, while the other end is kept adiabatic, as illustrated in Fig. 4. The goal is to determine the PCM's temperature distribution as a function of time and space. Since an exact analytical solution exists for this problem [55], it can be compared with the numerical procedure used in this investigation for validating the model. This investigation solved Stefan's problem for a 10 mm thick PCM having identical thermo-physical properties (given in Table 1) as those used in this investigation and a melting temperature of 26 °C, with its boundary temperature fixed at 50 °C. The only difference between the two PCMs was that in Stefan's problem, the PCM changed phase between a temperature range of 0.05 °C (26 °C–26.05 °C), while the PCM studied in the remainder of this investigation had a broader phase change temperature range (2 °C). This was necessary since the analytical expression is only valid for a PCM with a zero phase change temperature range.

Fig. 5 a–b shows the temperature distribution in the PCM at different times obtained with the exact analytical expression and numerical model using coarse (6 nodes to model the PCM) and fine grids (11 nodes to model the PCM). Note that although both grids satisfied the criteria suggested by Tabares-Velasco et al. [54], only the numerical results obtained with the fine grid can be deemed satisfactory. Thus, this exercise demonstrated the importance of grid size for simulating the phase change process and validated the modeling approach.

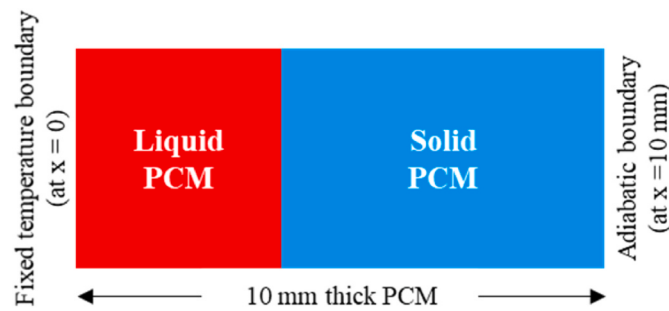
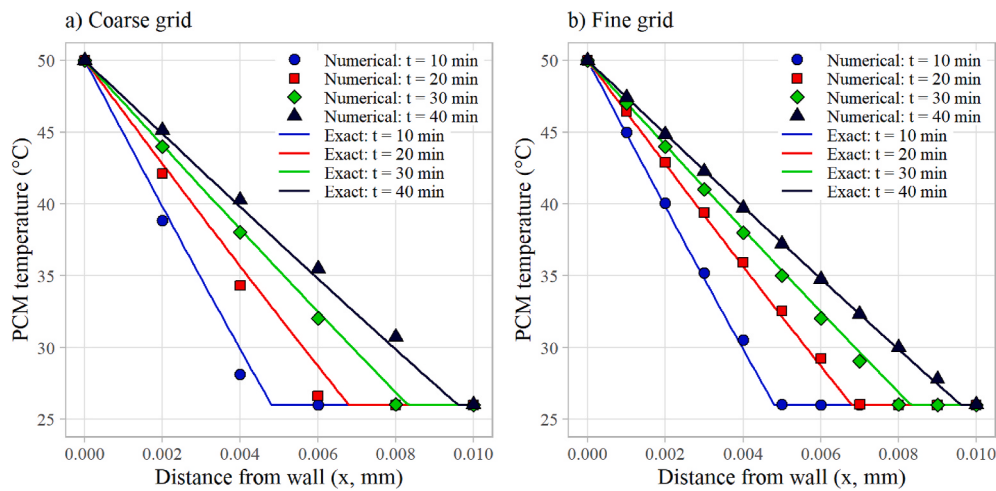


Fig. 4. Schematic of the Stefan's problem.



**Fig. 5.** Comparison between the temperature of the PCM at different spatial locations and time obtained with the exact analytical expression and the numerical model with a) coarse grid and b) fine grid.

### 2.6.2. Grid independence test

The comparison between the analytical results and numerical model for Stefan's problem indicated that a fine grid size would be appropriate for this study; however, that grid resolution led to large simulation times. Note that Stefan's problem deals with a PCM with a very narrow phase change temperature range ( $0.05\text{ }^{\circ}\text{C}$ ); however, the PCM integrated into building walls had a much broader phase change temperature range ( $2\text{ }^{\circ}\text{C}$ ) and subjected to very different boundary conditions. Thus, a grid independence analysis was performed to identify the appropriate grid size for this study. The results obtained with the two grid sizes were compared for a typical configuration (PCM-EPS-Brick configuration with a PCM melting temperature equal to  $42\text{ }^{\circ}\text{C}$ ). Fig. 6 shows the hourly variations of west wall heat gains obtained with both grids, which are clearly equal. Thus the coarse mesh was deemed appropriate for this investigation.

### 2.6.3. Energy balance analysis

To further ensure the validity of the results, this investigation also checked daily heat balances for all the simulations. Since periodic steady-state simulations were conducted, the total heat gained on the outer side of the wall during the day must be equal to the total heat loss on the inner side of the wall. The highest heat imbalance obtained was  $0.7\text{ Wh/m}^2$  (less than 2.8% errors), which was deemed reasonable for

this study, as given in Table SI 2. The Table also shows that heat imbalances were relatively high when the PCM was on the exterior surface of the wall (PCM-EPS-Brick and PCM-Brick-EPS), probably because those cases demonstrated the most intense melting and solidification cycles.

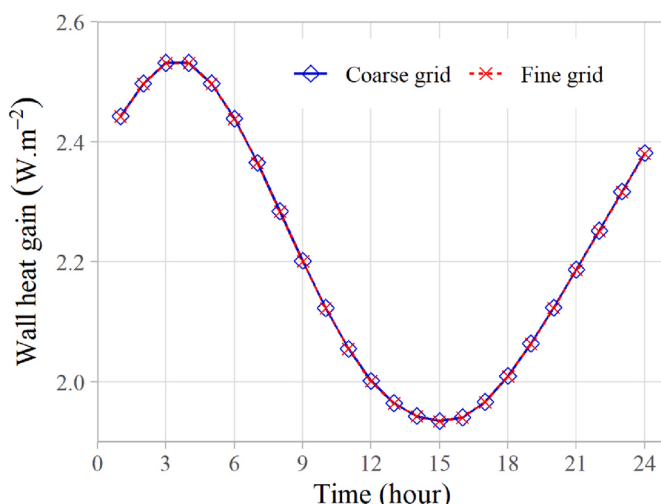
## 3. Results and discussion

To compare the energy performance of the different wall configurations, this investigation calculated the total daily heat gains (sum of hourly heat gains,  $\dot{q}_{HG,tot} = \int_{t=0}^{t=24\text{ h}} \dot{q}_{HG} dt$ ) and cooling loads (sum of hourly cooling loads,  $\dot{q}_{CL,tot} = \int_{t=0}^{t=24\text{ h}} \dot{q}_{CL} dt$ ) together with their peak (maximum) values. This section first describes the benefits obtained by integrating insulation in the standard wall by comparing the performance of Brick, Brick-EPS, and EPS-Brick walls shown in Fig. 1. Next, further potential benefits of PCM integration are explored by comparing insulated walls with the six different wall configurations that contain both PCM and insulation. Finally, the effect of night ventilation on cooling load reduction is discussed for the different wall configurations.

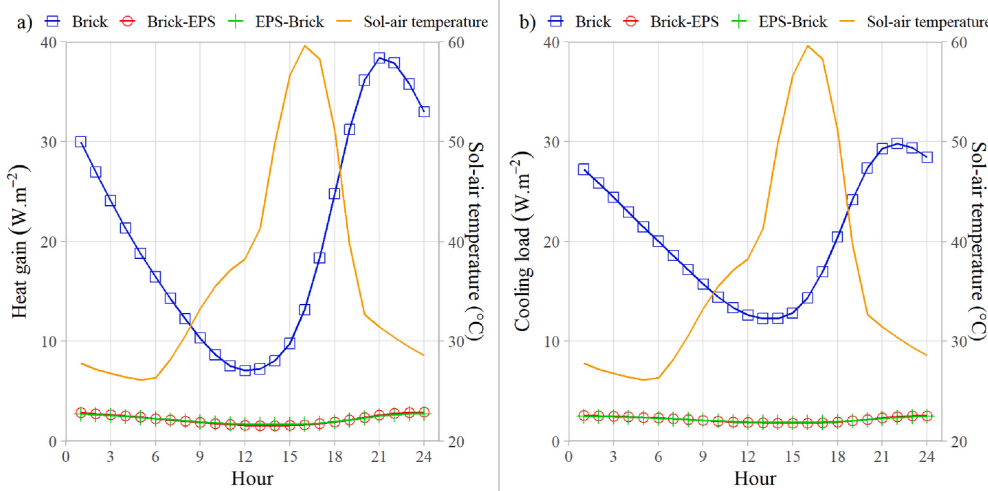
### 3.1. Effect of insulation

Fig. 7 a–b shows the hourly variations of heat gains and cooling loads for the standard brick wall (Brick) and for those modified with 150 mm thick EPS insulation layers on the inner side (Brick-EPS) or outer side (EPS-Brick) under T32R12 outdoor DBT conditions (see Fig. 3). As shown in the figure, these west-facing walls were subjected to intense solar radiation during the afternoon hours (sol-air temperature peaked at 16th hour), leading to high heat gains and cooling loads for the standard brick wall. Applying EPS insulation to the standard brick wall (Brick-EPS or EPS-Brick) reduced the total daily heat gain and cooling load by 89.4%. Similar reductions in daily heat gains and cooling loads (ranging from 84.4% to 89.4%) were obtained by applying wall insulation for other facing directions and outdoor DBT conditions (see Tables SI 3–4). Note that the total daily heat gains and cooling loads were equal in magnitude for each wall configuration due to periodic steady-state simulations; however, cooling load fluctuations were lower than those in heat gains due to the building's thermal mass.

Fig. 7 a–b also shows that applying insulation to the standard brick wall substantially reduced and delayed the peak heat gains and cooling loads. The peak heat gains and cooling loads were reduced by 90.3%–94.3% and 89.9%–93.1%, respectively, depending on the wall



**Fig. 6.** Comparison between hourly variations in wall heat gains obtained with coarse and fine grids for the PCM-EPS-Brick configuration.



**Fig. 7.** Comparison between hourly variations of a) heat gains and b) cooling loads of west-facing walls with Brick, Brick-EPS, and EPS-Brick configurations for the T32R12 outdoor DBT condition.

configuration, orientation, and outdoor DBT conditions, as given in Tables SI 5–6. The delays in peak heat gains and cooling load ranged from 1 to 5 h and 1–7 h, respectively, as given in Table SI 7–8. The reported performance benefits agreed with several previous investigations that have highlighted the tremendous potential of applying wall insulation for reducing the cooling loads [56,57]. It is also important to emphasize that the reported reductions in heat gains and cooling loads only accounted for their components due to wall heat transfer. The other heat gain and cooling load components (e.g., infiltration, internal gains, etc.) will remain unaffected by changes in the wall construction. The obtained results are useful since they set a baseline for assessing the performance of PCM-enhanced walls, as discussed in the next section.

### 3.2. Effect of PCM

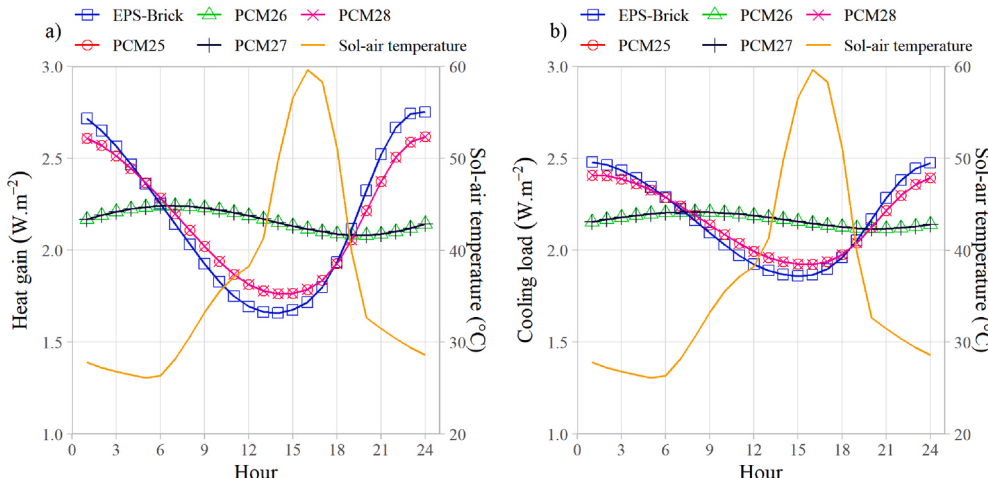
This research explored the additional benefits that could be obtained by integrating a PCM layer in addition to the EPS insulation through the various configurations that contained both insulation and PCM (see Fig. 1). This section first reports the results obtained when the PCM was placed on the inner side of the wall (EPS-Brick-PCM and Brick-EPS-PCM). This is followed by results obtained for cases when the PCM was sandwiched between the insulation and brick layers (EPS-PCM-Brick and Brick-PCM-EPS). Finally, results are presented for those

configurations in which the PCM was on the outer side of the wall (PCM-EPS-Brick and PCM-Brick-EPS).

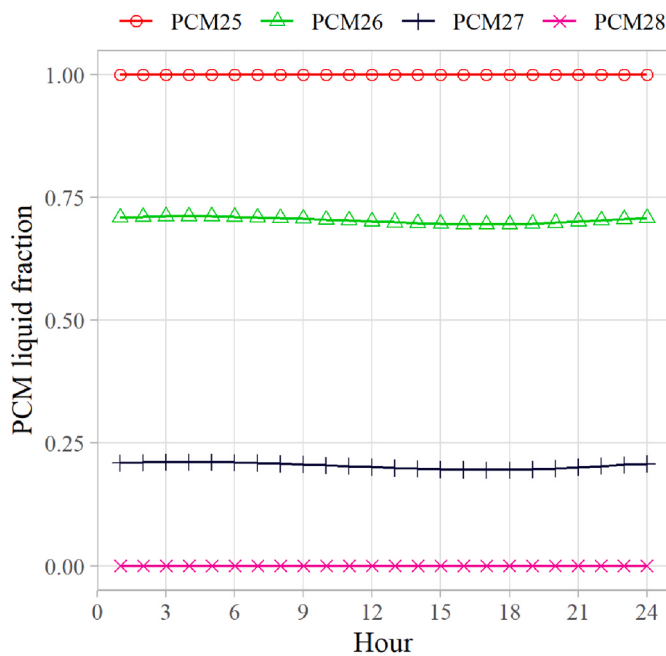
#### 3.2.1. PCM is the inner layer (EPS-brick-PCM and brick-EPS-PCM)

Fig. 8 a–b shows the comparison of hourly heat gains and cooling loads for west-facing walls subjected to T32R12 outdoor DBT profile for the EPS-Brick and EPS-Brick-PCM configurations. The west-facing wall under the T32R12 profile was taken as a representative case since it had the highest daily heat gains and cooling loads than walls facing other directions and DBT profiles, for which the results are given in the Supplementary Material. The numbers in the figure's legend (and for subsequent figures) after PCM denote its melting temperature in  $^{\circ}\text{C}$ , which means that for the EPS-Brick-PCM configuration, PCM26 represents this configuration with a PCM having 26  $^{\circ}\text{C}$  as its melting temperature. It is clear from the figure that with the addition of a PCM layer with an appropriate melting temperature (only PCM26 and PCM27 undergo phase change, as shown in Fig. 9), fluctuations in the hourly heat gains and cooling loads can be significantly damped. However, this did not lead to any reductions in the total daily heat gain or cooling load.

Fig. 9 shows the melt fractions for west-facing EPS-Brick-PCM walls subjected to the T32R12 DBT profile, which indicates that PCMs with melting temperatures lower than 25  $^{\circ}\text{C}$  or higher than 27  $^{\circ}\text{C}$  were inactive (did not undergo any phase transformation). The melt fractions



**Fig. 8.** Comparison between hourly variations of a) heat gains and b) cooling loads of west-facing walls with EPS-Brick and EPS-Brick-PCM (numbers in legend after PCM denote its melting temperature in  $^{\circ}\text{C}$ ) configurations for the T32R12 outdoor DBT condition.



**Fig. 9.** Hourly variations in PCM liquid fraction of west-facing EPS-Brick-PCM walls for the T32R12 outdoor DBT conditions.

for PCM26 and PCM27 increased from 5:00 p.m. to 4:00 a.m. (PCM melts) and decreased from 4:00 a.m. to 5:00 p.m. (PCM solidifies), as illustrated in Fig. 9. The PCMs remained in the 2-phase region (mixture of liquid and solid) throughout the day, meaning that the PCMs could not undergo a complete melting-solidification cycle, and only a tiny portion of their latent heats was utilized (3 kJ/kg out of 240 kJ/kg). The reason was that in this configuration, the PCM temperature remained close to the indoor set-point temperature ( $26^{\circ}\text{C}$ ) since the PCM was on the inner side of the wall, and the insulation and brick layers' thermal resistance shielded the PCM from outdoor temperature variations. Thus, the temperature difference across the PCM layer was very small throughout the day (less than  $0.2^{\circ}\text{C}$ ), which led to minimal heat transfer across it and thus little utilization of its latent heat. Furthermore, since the PCM temperature remained close to the indoor set-point temperature, only PCM26 and PCM27 were active in this configuration. The results for other outdoor DBT profiles (T32R6, T26R12, T26R6) and wall orientations (east, north, and south) were qualitatively similar to the results discussed above, as shown in Figs. SI 3–6. For the EPS-Brick-PCM configuration, when the PCM was active (PCM26 and PCM27), peak heat gains were reduced by 9.4%–43.5% and delayed by 6–7 h as compared to the EPS-Brick configuration, depending on the wall orientation and the outdoor DBT profile. Similarly, peak cooling loads were reduced by 5.8%–31.2% and delayed by 6–8 h due to the addition of the PCM.

For the Brick-EPS-PCM configuration, the hourly variations in heat gains, cooling loads, and PCM liquid fractions were qualitatively similar to those discussed above for the EPS-Brick-PCM configuration, as illustrated in Figs. SI 7–10. Similar to the EPS-Brick-PCM walls, the Brick-EPS-PCM walls also did not reduce the total daily heat gain or cooling load when compared with the EPS-Brick configuration. However, reductions in peak heat gains and peak cooling loads ranging from 9.9% to 45.2% and 5.8%–31.2%, respectively, were obtained depending on the wall orientation and the outdoor DBT profile. The peak heat gains and cooling loads shifted by 7–9 h and 8–9 h, respectively.

It is noteworthy that in both configurations (EPS-Brick-PCM, Brick-EPS-PCM), only PCMs with melting temperatures of  $26^{\circ}\text{C}$  or  $27^{\circ}\text{C}$  were active, irrespective of the outdoor conditions. This happened because the PCM was the innermost layer and shielded from outdoor conditions due to the insulation and brick layers' thermal resistance, as

discussed previously. Thus, it seems that for such wall configurations, the PCM melting temperature should be close to the indoor set-point temperature for utilizing its latent heat capacity, irrespective of outdoor conditions. Furthermore, since only a tiny fraction of the latent heat was used, a PCM with a much smaller latent heat should also produce a similar effect.

### 3.2.2. PCM layer is between brick and insulation layers (EPS-PCM-Brick and Brick-PCM-EPS)

For the EPS-PCM-Brick configuration, results were similar to the previously analyzed configurations since the PCM was shielded from outdoor conditions by the thick insulation layer (see Figs. SI 11–14). To summarize, in this configuration also, PCM26 and PCM27 were active. No reductions in total daily heat gains or cooling loads were obtained when compared to the EPS-Brick configuration. The peak heat gains and cooling load were reduced by 9.9%–45.2% and 5.8%–31.2%, respectively, depending on the wall orientation and the outdoor DBT profile. The peak heat gains and cooling loads were shifted by 4–6 h and 4–7 h, respectively.

For the Brick-PCM-EPS configuration, Fig. 10 shows the hourly variations in heat gains and cooling loads with PCMs of different melting temperatures for a west-facing wall subjected to T32R12 outdoor DBT conditions, which were qualitatively similar to the ones discussed previously. The heat gains and cooling load profiles were qualitatively similar for other facing directions and outdoor DBT profiles (see Figs. SI 15–18). One aspect where the Brick-PCM-EPS configuration differed from those discussed previously was that PCMs with higher melting temperatures ( $26^{\circ}\text{C}$ – $38^{\circ}\text{C}$ , depending on the wall orientation and outdoor DBT conditions) were active in this configuration. This was because the PCM was not shielded from outdoor conditions by the insulation layer. This behavior is illustrated in Fig. 11 for west-facing walls under the T32R12 DBT condition, and Figs. SI 15–18 for other orientations and outdoor DBT conditions. Notice that a relatively large portion of the PCM's latent heat was utilized for energy storage if its melting temperature was appropriate (81 kJ/kg out of 240 kJ/kg for PCM36, as shown in Fig. 11). However, no benefits were still obtained in terms of reductions in total daily heat gains or cooling loads.

With a PCM of appropriate melting temperature, the Brick-PCM-EPS configuration also reduced peak heat gains and peak cooling loads as compared to the EPS-Brick configuration, ranging between 9.9%–43.5% and 5.8%–31.2%, respectively, depending on the wall orientation and the outdoor DBT profile. For example, for the west wall shown in Fig. 11, PCM36 was appropriate since it led to the maximum utilization of latent heat. A proper selection of the PCM's melting temperature also delayed the peak heat gains and cooling loads by 2–6 h and 1–7 h, respectively. In situations when the PCM had an inappropriate melting temperature (PCM did not undergo phase change), the peak heat gains and cooling loads increased in this configuration by as much as 7.1% and 6.3%, respectively, when compared to the EPS-Brick wall. This happened because the Brick-PCM-EPS wall had insulation on the inner side, which led to overheating of the outer brick and PCM layers during the day and resulted in higher peak heat gains and cooling loads, as compared to the EPS-Brick wall that had outer insulation. Those results agreed with previous research, which demonstrated that under periodic steady-state conditions, placing the insulation near the inner surface of the wall resulted in a higher peak load as compared to placing it near the outer surface [58]. No delays in peak heat gains or cooling loads were observed in such cases (Brick-PCM-EPS configuration with inactive PCM). Therefore, in this configuration, it is essential to choose a PCM with a suitable melting temperature; otherwise, the performance of this wall will be inferior to the EPS-Brick wall in terms of peak heat gains and cooling loads.

### 3.2.3. PCM is the outer layer (PCM-EPS-brick and PCM-brick-EPS)

Fig. 12 a–b shows the daily variations in west wall heat gains and cooling loads for the PCM-EPS-Brick wall with T32R12 DBT profile,

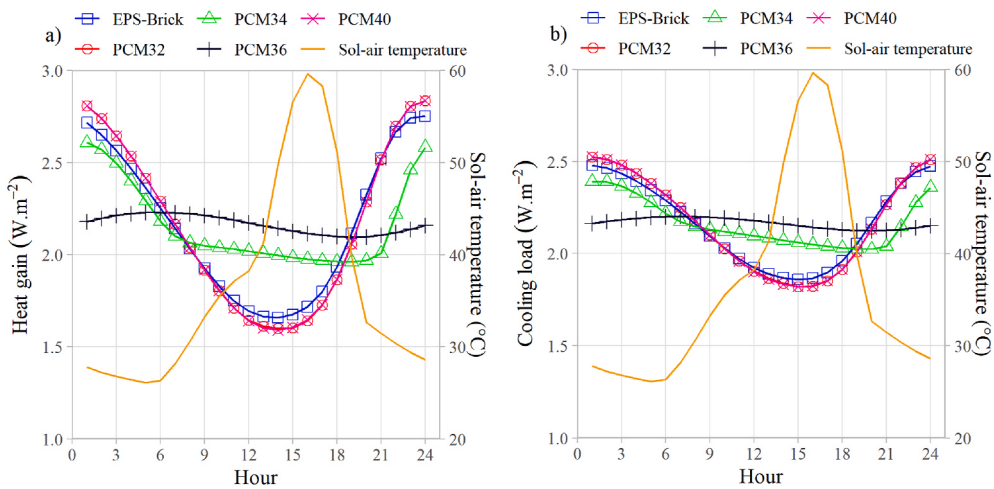


**Fig. 10.** Comparison between hourly variations of a) heat gains and b) cooling loads of west-facing walls with EPS-Brick and Brick-PCM-EPS (numbers in legend after PCM denote its melting temperature in °C) configurations for the T32R12 outdoor DBT condition.

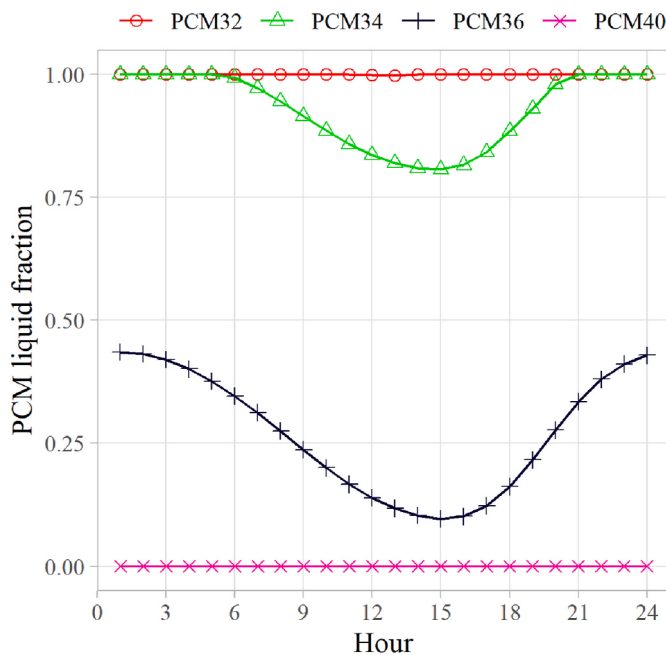


**Fig. 11.** Hourly variations in PCM liquid fraction of west-facing Brick-PCM-EPS walls for the T32R12 outdoor DBT conditions.

which were qualitatively similar to the results discussed previously. The PCM underwent complete melting-solidification cycles, when its melting temperature was appropriate, as shown in Fig. 13, but still, no reductions were obtained in the total daily heat gains and cooling loads with this configuration when compared to the EPS-Brick configuration. The hourly variations in heat gains, cooling loads, and melt fractions for this wall configuration with other orientations and outdoor DBT profiles were similar to those discussed above (see Figs. SI 19–22). Note that, in this configuration, the PCM was active over melting temperatures ranging from 26 °C–56 °C, which is about the same as the daily variation in the sol-air temperature. This configuration also reduced and delayed the peak heat gains and cooling loads as compared to the EPS-Brick wall, when a PCM with a suitable melting temperature was chosen. In those cases, reductions in peak heat gains and cooling loads ranged from 9.9% to 40.3% and 5.7%–29.2%, respectively, and their delays were between 1 and 9 h, depending on the wall orientation and DBT profile. In cases when the PCM did not have an appropriate melting temperature, this

configuration did not lead to any increase in the peak heat gains or cooling loads, unlike the Brick-PCM-EPS configuration.

The results for the PCM-Brick-EPS configuration were quite similar to the PCM-EPS-Brick configuration since both of them had PCM on the outer side, as illustrated in Figs. SI 23–26. However, for the PCM-Brick-EPS configuration, the PCM was active over a narrower range of melting temperatures than the PCM-EPS-Brick configuration. This happened because the PCM-Brick-EPS wall had the brick layer next to the PCM, which allowed heat transfer from the PCM to the wall's inner region, and thereby lowered the PCM temperature as compared to that in the PCM-EPS-Brick configuration. The PCM-Brick-EPS configuration also did not reduce the total daily heat gains or cooling loads compared to the EPS-Brick configuration. When the PCM's melting temperature was appropriate, this configuration also decreased peak heat gains and cooling loads ranging from 8.8% to 37.1% and 5.2%–25.0%, respectively, compared to the EPS-Brick configuration for different wall orientations and DBT profiles. The corresponding delays ranged from 2 to 7 h and 4–7 h for heat gains and cooling loads, respectively. No detrimental effect was found when the PCM's melting temperature was inappropriate.

To summarize, this investigation compared the thermal performance of insulated walls (2 configurations) with those containing both insulation and PCM (6 configurations) facing four different cardinal directions under four distinct outdoor air DBT profiles, i.e., a total of 128 (8 × 4 × 4) unique cases. Additionally, the PCM's melting temperature was also varied, which further increased the number of analyzed cases. Remarkably, the total daily heat gains and cooling loads were equal for all these eight configurations (all configurations had identical thermal resistance but significantly different thermal masses) when subjected to identical boundary conditions. The total daily heat gains or cooling loads could be predicted (within 2.5% error) from simple steady-state

considerations by using  $\dot{q}_{HG,tot} = \dot{q}_{CL,tot} = U \sum_{n=1}^{n=24} (T_{sol-air,n} - T_{in})$ , where  $U$  denotes the overall heat transfer coefficient between the outdoor and indoor air.

The hourly variations in heat gains were significantly damped due to the integration of the PCM, as shown in Fig. 14 a–b. The figure clearly shows that as higher amounts of the PCM's latent heat were utilized for a particular wall configuration, the maximum (peak) heat gains were reduced. At the same time, the minimum increased until their values were almost equal. Similar results were obtained with other outdoor DBT conditions and wall orientations as well. There are small fluctuations in the curves for specific configurations, which are likely numerical artifacts. Those results also agreed with Tsilingiris [59], who assessed

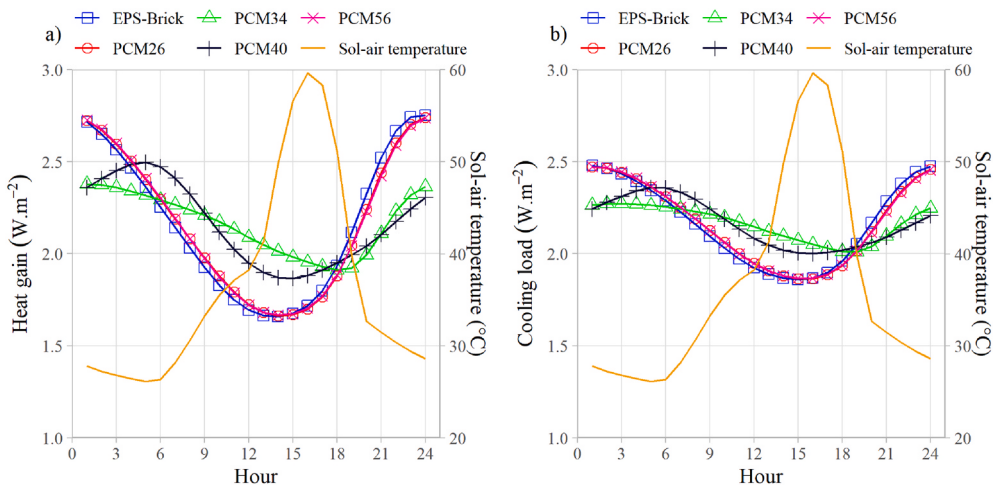


**Fig. 12.** Comparison between hourly variations of a) heat gains and b) cooling loads of west-facing walls with EPS-Brick and PCM-EPS-Brick (numbers in legend after PCM denote its melting temperature in  $^{\circ}\text{C}$ ) configurations for the T32R12 outdoor DBT condition.

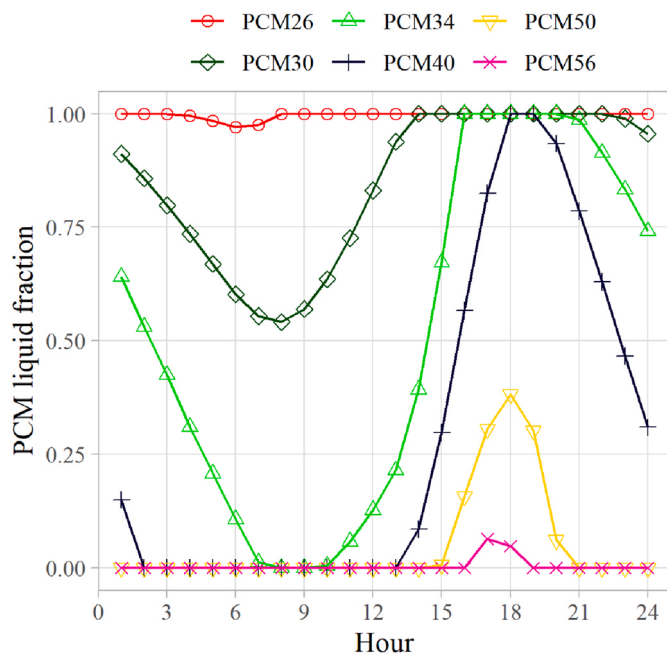


**Fig. 13.** Hourly variations in PCM liquid fraction of west-facing PCM-EPS-Brick walls for the T32R12 outdoor DBT conditions.

the influence of heat capacity on the thermal behavior of walls subjected to periodic steady-state conditions, and reported that an increase in wall heat capacity only damped the temporal variations in heat flux, but did not affect the total daily heat gains.

### 3.3. Effect of night ventilation

This section further assessed the potential benefits of the proposed wall enhancement techniques with the incorporation of night ventilation. The effect of night ventilation on the energy performance of the different wall configurations was studied for the T26R12 (a mild summer day with  $T_{avg} = 26^{\circ}\text{C}$  and  $12^{\circ}\text{C}$  difference between the maximum and minimum temperature) DBT profile only since this profile was most suited for implementing night ventilation. Note that the night ventilation rates (obtained from Eq. (10)) represent the required ventilation to offset the wall cooling loads completely. Thus, the cooling loads reported in this section are their minimum values when night ventilation is

a feasible ‘free’ cooling strategy. However, in real residential buildings, the ventilation rates will be significantly different from those obtained by Eq. (10), which will lead to the actual wall cooling loads deviating from the values reported here. Nevertheless, this section reports the energy performance of the different wall configurations under ventilation rates that are best suited for that particular configuration. Thus, it provides a fair comparison between the maximum energy-saving potential of insulation and PCM-based wall enhancement strategies in the presence of night ventilation.

Fig. 15 a–b shows the hourly variations in cooling loads with and without night ventilation for west-facing Brick and EPS-Brick walls, along with the outdoor air DBTs and required night ventilation rates, as calculated from Eq. (10). As illustrated in the figure, night ventilation was suitable from 8:00 p.m. to 9:00 a.m. (21st hour to 9th hour) when the outdoor air temperatures were lower than the indoor set-point temperature ( $26^{\circ}\text{C}$ ). This meant that cooling loads were zero during those hours due to the ‘free’ cooling provided by outdoor air. The ventilation rates required for ‘free’ cooling were significantly lower for the EPS-Brick wall than those for the standard Brick wall since the hourly cooling loads were much smaller for the EPS-Brick wall. For Brick-EPS walls, applying night ventilation led to hourly cooling loads and ventilation rates that were very similar to those for the EPS-Brick configuration, as shown in Fig. SI 27 for a west-facing wall. For walls facing other directions, the hourly cooling loads and required night ventilation rates were qualitatively similar to those discussed above.

For all the wall configurations, the cooling loads significantly reduced due to the application of night ventilation, ranging from 50% to 103%, 58%–70%, and 58%–73% for the Brick, EPS-Brick, and Brick-EPS walls, respectively, depending on the wall orientation, as shown in Fig. 16. As evident from the figure, insulated walls (EPS-Brick or Brick-EPS) with night ventilation led to the lowest cooling loads for all orientations except north, for which the standard Brick wall had the lowest (negative) cooling load. The negative load meant that with sufficient night ventilation rates, a north-facing Brick wall led to a net heat loss from the air-conditioned zone, and insulating it would slightly deteriorate the wall’s energy performance. This finding is corroborated by Kolaitis et al. [60], who reported that wall insulation could *increase* the cooling loads due to its preventing the night-time ‘free’ cooling effect.

This investigation also compared the daily cooling load requirements of the various PCM-enhanced walls to those for the insulated walls (Brick-EPS and EPS-Brick) with the application of night ventilation, as shown in Fig. 17. For PCM-enhanced configurations shown in Fig. 17, the PCM’s melting temperature was selected to maximize its latent heat storage, and for those configurations that had multiple such temperatures, the average cooling load across all such temperatures were

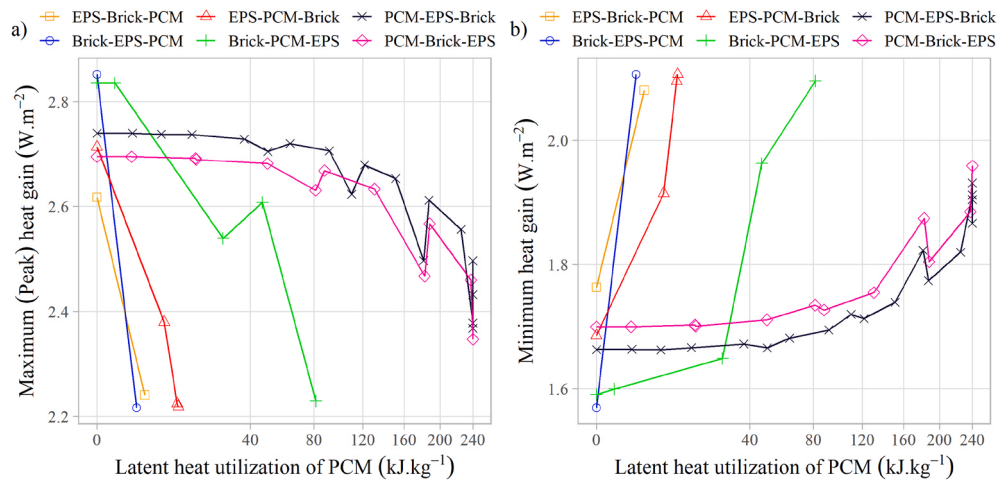


**Fig. 14.** Effect of PCM's latent heat utilization on the a) maximum and b) minimum heat gains through different west-facing wall configurations for T32R12 outdoor DBT conditions.

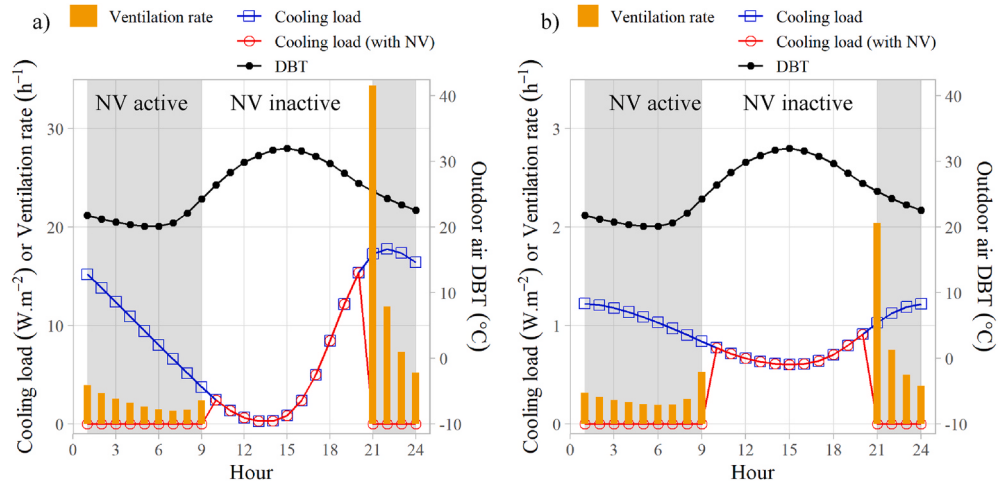


**Fig. 15.** Comparison between hourly variations of cooling loads for a) Brick and b) EPS-Brick walls for T32R12 outdoor DBT conditions with and without night ventilation (NV).

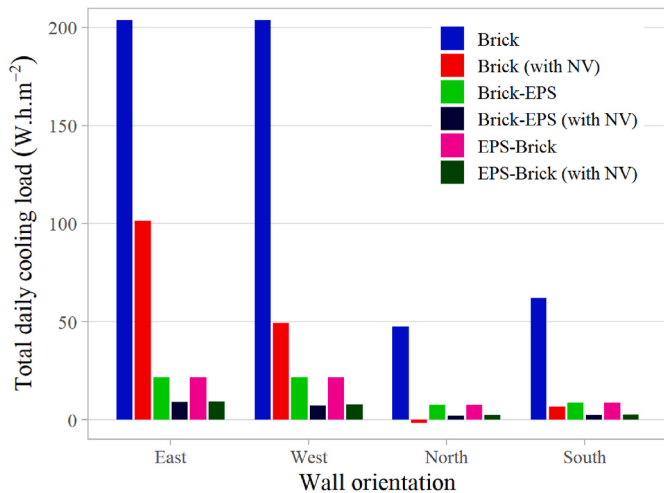


**Fig. 16.** Comparison between cooling load requirements for Brick, Brick-EPS, and EPS-Brick walls with and without night ventilation (NV) for different wall orientations.

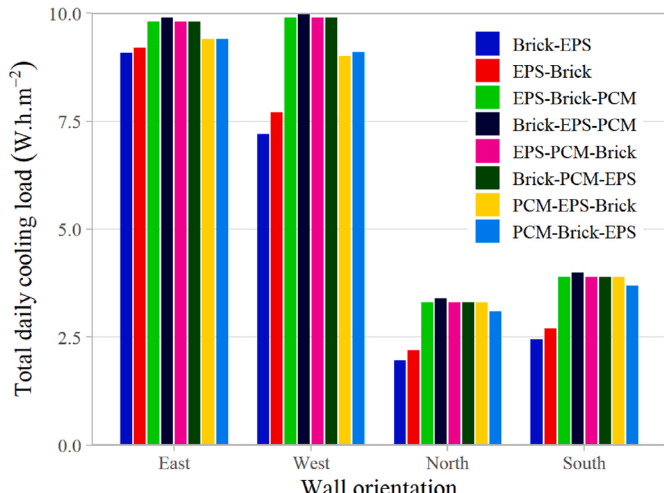


**Fig. 17.** Comparison between cooling load requirements for walls enhanced with insulation only and those enhanced with both insulation and PCM for different orientations in the presence of night ventilation.

plotted. As shown in the figure, EPS-Brick walls had slightly higher cooling loads (by 0.1–0.5 W h m<sup>-2</sup>, depending on the wall orientation) than the Brick-EPS walls for all orientations. The cooling loads increased with PCM integration, and were 2%–53% higher for PCM-enhanced walls than those for EPS-Brick walls, depending on the wall configuration and orientation. Thus, even after employing night ventilation, PCM integration into a well-insulated wall did not produce any reductions in the daily cooling load.

It must be highlighted that utmost care was taken to ensure the reliability of the numerical simulations reported in this investigation, as evident from the three different tests used for model validation (see Section 2.6). The simulation conditions in this study were selected not to represent a particular building type or climate zone precisely, but rather to compare the energy performance of different configurations of PCM-enhanced heavyweight walls under ‘typical’ conditions while keeping their thermal resistances equal. Thus, the results help make a fair assessment of the impact of latent heat storage by the PCM on the cooling energy requirements of different configurations of PCM-enhanced walls, which is seldom possible in real-world case studies.

#### 4. Conclusions

This investigation numerically studied the periodic steady-state behavior of one-dimensional heat conduction through heavyweight residential walls enhanced with PCM and insulation layers arranged in different configurations. The walls were exposed to sixteen different solar air temperature profiles to represent various outdoor conditions on a typical summer day, while the indoor temperature was maintained constant at 26 °C. The energy performance of those walls was compared to walls enhanced only with an insulation layer under identical conditions while maintaining equal thermal resistances. The study led to the following conclusions:

- The total daily heat gains and cooling loads were equal for all the different wall configurations with equal thermal resistances when subjected to identical boundary conditions, regardless of the amount of latent heat stored by the PCM layer. However, the latent heat stored by the PCM reduced the fluctuations in the hourly heat gains and cooling loads. Thus, PCM integration was ineffective in reducing the daily heat gains or the cooling load requirements, although it seems suitable for peak load management.
- The utilization of PCM’s latent heat depended on its melting temperature and its positioning in the wall. When a PCM of the appropriate melting temperature was selected, the least amount of latent heat got utilized when the PCM was shielded from outdoor conditions by the insulation layer. In contrast, the maximum amount of latent heat was used when the PCM was directly exposed to outdoor conditions.
- It is recommended to position the PCM layer on the inner side of the wall with sufficient insulation shielding it from outdoor conditions. In such a configuration, the PCM’s melting temperature should be equal to or slightly higher than the indoor set-point temperature for utilizing its latent heat capacity. Furthermore, in this configuration, a PCM of relatively low latent heat capacity can be used since the PCM would be shielded from outdoor conditions, thereby experiencing low heat transfer across it.
- The application of night ventilation significantly reduced the cooling loads across all wall configurations due to the ‘free’ cooling provided by the cold outdoor air at night-time. However, even after employing night ventilation, the addition of PCM to a well-insulated wall did not lead to any benefits in terms of reducing the total daily cooling load.

#### Funding

This study was supported by Birla Institute of Technology and

Science (BITS), Pilani, through its Outstanding Potential for Excellence in Research and Academics (OPERA) award.

#### Declaration of competing interest

The authors declare that they have no known competing financial interests or personal relationships that could have appeared to influence the work reported in this paper.

#### Appendix A. Supplementary data

Supplementary data to this article can be found online at <https://doi.org/10.1016/j.buildenv.2021.107930>.

#### References

- [1] IPCC (Intergovernmental Panel on Climate Change), Climate Change 2014: Mitigation of Climate Change; Working Group III Contribution to the Fifth Assessment Report of the Intergovernmental Panel on Climate Change, Cambridge Univ. Press, New York, NY, 2014.
- [2] M. Isaac, D.P. van Vuuren, Modeling global residential sector energy demand for heating and air conditioning in the context of climate change, Energy Pol. 37 (2009) 507–521, <https://doi.org/10.1016/j.enpol.2008.09.051>.
- [3] H. Akeiber, P. Nejat, M.Z. Abd Majid, M.A. Wahid, F. Jomehzadeh, I. Zeynali Famileh, J.K. Calautti, B.R. Hughes, S.A. Zaki, A review on phase change material (PCM) for sustainable passive cooling in building envelopes, Renew. Sustain. Energy Rev. 60 (2016) 1470–1497, <https://doi.org/10.1016/j.rser.2016.03.036>.
- [4] F. Kuznik, D. David, K. Johannes, J.-J. Roux, A review on phase change materials integrated in building walls, Renew. Sustain. Energy Rev. 15 (2011) 379–391, <https://doi.org/10.1016/j.rser.2010.08.019>.
- [5] Z. Liu, Z. (Jerry) Yu, T. Yang, D. Qin, S. Li, G. Zhang, F. Haghighat, M.M. Joybari, A review on macro-encapsulated phase change material for building envelope applications, Build. Environ. 144 (2018) 281–294, <https://doi.org/10.1016/j.buildenv.2018.08.030>.
- [6] F. Souayfane, F. Fardoun, P.-H. Biwole, Phase change materials (PCM) for cooling applications in buildings: a review, Energy Build. 129 (2016) 396–431, <https://doi.org/10.1016/j.enbuild.2016.04.006>.
- [7] M.A. Wahid, S.E. Hosseini, H.M. Hussen, H.J. Akeiber, S.N. Saud, A. Th Mohammad, An overview of phase change materials for construction architecture thermal management in hot and dry climate region, Appl. Therm. Eng. 112 (2017) 1240–1259, <https://doi.org/10.1016/j.applthermaleng.2016.07.032>.
- [8] Y. Zhou, S. Zheng, G. Zhang, A review on cooling performance enhancement for phase change materials integrated systems—flexible design and smart control with machine learning applications, Build. Environ. 174 (2020) 106786, <https://doi.org/10.1016/j.buildenv.2020.106786>.
- [9] F. Mathieu-Potvin, L. Gosselin, Thermal shielding of multilayer walls with phase change materials under different transient boundary conditions, Int. J. Therm. Sci. 48 (2009) 1707–1717, <https://doi.org/10.1016/j.ijthermalsci.2009.01.010>.
- [10] M. Saffari, A. de Gracia, S. Ushak, L.F. Cabeza, Passive cooling of buildings with phase change materials using whole-building energy simulation tools: a review, Renew. Sustain. Energy Rev. 80 (2017) 1239–1255, <https://doi.org/10.1016/j.rser.2017.05.139>.
- [11] D.E.M. Bond, W.W. Clark, M. Kimber, Configuring wall layers for improved insulation performance, Appl. Energy 112 (2013) 235–245, <https://doi.org/10.1016/j.apenergy.2013.06.024>.
- [12] A. Fateh, D. Borelli, F. Devia, H. Weinläder, Summer thermal performances of PCM-integrated insulation layers for light-weight building walls: effect of orientation and melting point temperature, Therm. Sci. Eng. Prog. 6 (2018) 361–369, <https://doi.org/10.1016/j.tsep.2017.12.012>.
- [13] J.C. Lam, Residential sector air conditioning loads and electricity use in Hong Kong, Energy Convers. Manag. 41 (2000) 1757–1768, [https://doi.org/10.1016/S0196-8904\(00\)00018-2](https://doi.org/10.1016/S0196-8904(00)00018-2).
- [14] M. Shekarchian, M. Moghavemi, B. Rismanchi, T.M.I. Mahlia, T. Olofsson, The cost benefit analysis and potential emission reduction evaluation of applying wall insulation for buildings in Malaysia, Renew. Sustain. Energy Rev. 16 (2012) 4708–4718, <https://doi.org/10.1016/j.rser.2012.04.045>.
- [15] P. Saikia, M. Pancholi, D. Sood, D. Rakshit, Dynamic optimization of multi-retrofit building envelope for enhanced energy performance with a case study in hot Indian climate, Energy 197 (2020) 117263, <https://doi.org/10.1016/j.energy.2020.117263>.
- [16] X. Sun, J. Jovanovic, Y. Zhang, S. Fan, Y. Chu, Y. Mo, S. Liao, Use of encapsulated phase change materials in lightweight building walls for annual thermal regulation, Energy 180 (2019) 858–872, <https://doi.org/10.1016/j.energy.2019.05.112>.
- [17] A.C. Evers, M.A. Medina, Y. Fang, Evaluation of the thermal performance of frame walls enhanced with paraffin and hydrated salt phase change materials using a dynamic wall simulator, Build. Environ. 45 (2010) 1762–1768, <https://doi.org/10.1016/j.buildenv.2010.02.002>.
- [18] X. Jin, M.A. Medina, X. Zhang, On the placement of a phase change material thermal shield within the cavity of buildings walls for heat transfer rate reduction, Energy 73 (2014) 780–786, <https://doi.org/10.1016/j.energy.2014.06.079>.

- [19] X. Sun, M.A. Medina, K.O. Lee, X. Jin, Laboratory assessment of residential building walls containing pipe-encapsulated phase change materials for thermal management, Energy 163 (2018) 383–391, <https://doi.org/10.1016/j.energy.2018.08.159>.
- [20] K.O. Lee, M.A. Medina, X. Sun, X. Jin, Thermal performance of phase change materials (PCM)-enhanced cellulose insulation in passive solar residential building walls, Sol. Energy 163 (2018) 113–121, <https://doi.org/10.1016/j.solener.2018.01.086>.
- [21] K.O. Lee, M.A. Medina, E. Raith, X. Sun, Assessing the integration of a thin phase change material (PCM) layer in a residential building wall for heat transfer reduction and management, Appl. Energy 137 (2015) 699–706, <https://doi.org/10.1016/j.apenergy.2014.09.003>.
- [22] M. Medina, J. King, M. Zhang, On the heat transfer rate reduction of structural insulated panels (SIPs) outfitted with phase change materials (PCMs), Energy 33 (2008) 667–678, <https://doi.org/10.1016/j.energy.2007.11.003>.
- [23] X. Sun, M.A. Medina, Y. Zhang, Potential thermal enhancement of lightweight building walls derived from using Phase Change Materials (PCMs), Front. Energy Res. 7 (2019), <https://doi.org/10.3389/fenrg.2019.00013>.
- [24] M. Alam, H. Jamil, J. Sanjayan, J. Wilson, Energy saving potential of phase change materials in major Australian cities, Energy Build. 78 (2014) 192–201, <https://doi.org/10.1016/j.enbuild.2014.04.027>.
- [25] A. Fateh, F. Klinker, M. Brüttig, H. Weinläder, F. Devia, Numerical and experimental investigation of an insulation layer with phase change materials (PCMs), Energy Build. 153 (2017) 231–240, <https://doi.org/10.1016/j.enbuild.2017.08.007>.
- [26] C.K. Halford, R.F. Boehm, Modeling of phase change material peak load shifting, Energy Build. 39 (2007) 298–305, <https://doi.org/10.1016/j.enbuild.2006.07.005>.
- [27] K.O. Lee, M.A. Medina, Using phase change materials for residential air conditioning peak demand reduction and energy conservation in coastal and transitional climates in the State of California, Energy Build. 116 (2016) 69–77, <https://doi.org/10.1016/j.enbuild.2015.12.012>.
- [28] S.M. Sajjadi, J. Lewis, S. Sharples, The potential of phase change materials to reduce domestic cooling energy loads for current and future UK climates, Energy Build. 93 (2015) 83–89, <https://doi.org/10.1016/j.enbuild.2015.02.029>.
- [29] N. Soares, A.R. Gaspar, P. Santos, J.J. Costa, Multi-dimensional optimization of the incorporation of PCM-drywalls in lightweight steel-framed residential buildings in different climates, Energy Build. 70 (2014) 411–421, <https://doi.org/10.1016/j.enbuild.2013.11.072>.
- [30] S.D. Zwanzig, Y. Lian, E.G. Brehob, Numerical simulation of phase change material composite wallboard in a multi-layered building envelope, Energy Convers. Manag. 69 (2013) 27–40, <https://doi.org/10.1016/j.enconman.2013.02.003>.
- [31] R.A. Kishore, M.V.A. Bianchi, C. Booten, J. Vidal, R. Jackson, Modulating thermal load through lightweight residential building walls using thermal energy storage and controlled precooling strategy, Appl. Therm. Eng. 180 (2020) 115870, <https://doi.org/10.1016/j.applthermaleng.2020.115870>.
- [32] E. Solgi, Z. Hamedani, R. Fernando, B. Mohammad Kari, A parametric study of phase change material characteristics when coupled with thermal insulation for different Australian climatic zones, Build. Environ. 163 (2019) 106317, <https://doi.org/10.1016/j.buildenv.2019.106317>.
- [33] E. Solgi, Z. Hamedani, R. Fernando, B. Mohammad Kari, H. Skates, A parametric study of phase change material behaviour when used with night ventilation in different climatic zones, Build. Environ. 147 (2019) 327–336, <https://doi.org/10.1016/j.buildenv.2018.10.031>.
- [34] F. Ascione, N. Bianco, R.F. De Masi, F. de' Rossi, G.P. Vanoli, Energy refurbishment of existing buildings through the use of phase change materials: energy savings and indoor comfort in the cooling season, Appl. Energy 113 (2014) 990–1007, <https://doi.org/10.1016/j.apenergy.2013.08.045>.
- [35] A. Baniasadi, B. Sajadi, M. Amidpour, N. Noori, Economic optimization of PCM and insulation layer thickness in residential buildings, Sustain. Energy Technol. Assess. 14 (2016) 92–99, <https://doi.org/10.1016/j.seta.2016.01.008>.
- [36] M.A. Izquierdo-Barrientos, J.F. Belmonte, D. Rodríguez-Sánchez, A.E. Molina, J. A. Almendros-Ibáñez, A numerical study of external building walls containing phase change materials (PCM), Appl. Therm. Eng. 47 (2012) 73–85, <https://doi.org/10.1016/j.applthermaleng.2012.02.038>.
- [37] J. Lei, J. Yang, E.-H. Yang, Energy performance of building envelopes integrated with phase change materials for cooling load reduction in tropical Singapore, Appl. Energy 162 (2016) 207–217, <https://doi.org/10.1016/j.apenergy.2015.10.031>.
- [38] G.P. Panayiotou, S.A. Kalogirou, S.A. Tassou, Evaluation of the application of phase change materials (PCM) on the envelope of a typical dwelling in the Mediterranean region, Renew. Energy 97 (2016) 24–32, <https://doi.org/10.1016/j.renene.2016.05.043>.
- [39] N. Soares, C.F. Reinhart, A. Hajiah, Simulation-based analysis of the use of PCM-wallboards to reduce cooling energy demand and peak-loads in low-rise residential heavyweight buildings in Kuwait, Build. Simul. 10 (2017) 481–495, <https://doi.org/10.1007/s12273-017-0347-2>.
- [40] R. Vicente, T. Silva, Brick masonry walls with PCM macrocapsules: an experimental approach, Appl. Therm. Eng. 67 (2014) 24–34, <https://doi.org/10.1016/j.applthermaleng.2014.02.069>.
- [41] R. Saxena, K. Biplab, D. Rakshit, Quantitative assessment of phase change material utilization for building cooling load abatement in composite climatic condition, J. Sol. Energy Eng. 140 (2018), <https://doi.org/10.1115/1.4038047>.
- [42] M. Arici, F. Bilgin, S. Nižetić, H. Karabay, PCM integrated to external building walls: an optimization study on maximum activation of latent heat, Appl. Therm. Eng. 165 (2020) 114560, <https://doi.org/10.1016/j.applthermaleng.2019.114560>.
- [43] E. Tunçbilek, M. Arici, M. Krajcík, S. Nižetić, H. Karabay, Thermal performance based optimization of an office wall containing PCM under intermittent cooling operation, Appl. Therm. Eng. 179 (2020) 115750, <https://doi.org/10.1016/j.applthermaleng.2020.115750>.
- [44] Viven Sharma, A.C. Rai, Performance assessment of residential building envelopes enhanced with phase change materials, Energy Build. 208 (2020), <https://doi.org/10.1016/j.enbuild.2019.109664>.
- [45] L.W. Davis, P.J. Gertler, Contribution of air conditioning adoption to future energy use under global warming, Proc. Natl. Acad. Sci. Unit. States Am. 112 (2015) 5962–5967, <https://doi.org/10.1073/pnas.1423558112>.
- [46] M. Li, Z. Wu, J. Tan, Heat storage properties of the cement mortar incorporated with composite phase change material, Appl. Energy 103 (2013) 393–399, <https://doi.org/10.1016/j.apenergy.2012.09.057>.
- [47] F.C. McQuiston, J.D. Parker, J.D. Spitler, Heating, Ventilating, and Air Conditioning: Analysis and Design, John Wiley & Sons, 2004.
- [48] F. Kuznik, J. Virgone, J. Noel, Optimization of a phase change material wallboard for building use, Appl. Therm. Eng. 28 (2008) 1291–1298, <https://doi.org/10.1016/j.applthermaleng.2007.10.012>.
- [49] E. Mohseni, W. Tang, Parametric analysis and optimisation of energy efficiency of a lightweight building integrated with different configurations and types of PCM, Renew. Energy 168 (2021) 865–877, <https://doi.org/10.1016/j.renene.2020.12.112>.
- [50] L.F. Cabeza, A. Castell, C. Barreneche, A. de Gracia, A.I. Fernández, Materials used as PCM in thermal energy storage in buildings: a review, Renew. Sustain. Energy Rev. 15 (2011) 1675–1695, <https://doi.org/10.1016/j.rser.2010.11.018>.
- [51] DoE (Department of Energy), EnergyPlus Version 9.0.1 Documentation, Engineering Reference, 2018. [https://energyplus.net/sites/all/modules/custum/nrel\\_custom/pdfs/pdfs\\_v9.0.1/EngineeringReference.pdf](https://energyplus.net/sites/all/modules/custum/nrel_custom/pdfs/pdfs_v9.0.1/EngineeringReference.pdf).
- [52] J.D. Spitler, D.E. Fisher, C.O. Pedersen, The radiant time series cooling load calculation procedure, ASHRAE Trans. 103 (1997) 503–515.
- [53] ASHRAE, (American Society of Heating, Refrigerating and Air-Conditioning Engineers), ASHRAE Fundamentals, Handbook, 2009.
- [54] P.C. Tabares-Velasco, C. Christensen, M. Bianchi, C. Booten, Verification and Validation of EnergyPlus Conduction Finite Difference and Phase Change Material Models for Opaque Wall Assemblies, National Renewable Energy Laboratory (NREL), Golden, CO (United States), 2012.
- [55] L.M. Jiji, Heat Convection, Springer, 2006.
- [56] Z. Fang, N. Li, B. Li, G. Luo, Y. Huang, The effect of building envelope insulation on cooling energy consumption in summer, Energy Build. 77 (2014) 197–205, <https://doi.org/10.1016/j.enbuild.2014.03.030>.
- [57] W.A. Friess, K. Rahshan, T.A. Hendawi, S. Tajerzadeh, Wall insulation measures for residential villas in Dubai: a case study in energy efficiency, Energy Build. 44 (2012) 26–32, <https://doi.org/10.1016/j.enbuild.2011.10.005>.
- [58] S.A. Al-Sanea, M.F. Zedan, Effect of insulation location on thermal performance of building walls under steady periodic conditions, Int. J. Ambient Energy 22 (2001) 59–72, <https://doi.org/10.1080/01430750.2001.9675389>.
- [59] P.T. Tsilingiris, The influence of heat capacity and its spatial distribution on the transient wall thermal behavior under the effect of harmonically time-varying driving forces, Build. Environ. 41 (2006) 590–601, <https://doi.org/10.1016/j.buildenv.2005.02.031>.
- [60] D.I. Kolaitis, E. Malliotakis, D.A. Kontogeorgos, I. Mandilaras, D.I. Katsourinis, M. A. Founti, Comparative assessment of internal and external thermal insulation systems for energy efficient retrofitting of residential buildings, Energy Build. 64 (2013) 123–131, <https://doi.org/10.1016/j.enbuild.2013.04.004>.